J. Am. Ceram. Soc., 99 [4] 1271–1279 (2016)
DOI: 10.1111/jace.14095

journal

Conductive and Radiative Properties of Soda-Lime Silicate Glassmelts with Different Iron Contents from 1100°C to 1500°C

Hua Liu,[‡] Rei Kitamura,[§] Xinlin Xia,[‡] and Laurent Pilon[¶,†]

[‡]Harbin Institute of Technology, School of Energy Science and Engineering, No. 92, West Dazhi Street, Harbin, Heilongjiang 150001, China

[§]Production Technology Center, Asahi Glass Corporation, Ltd, 1-1 Suehirocho, Tsurumi-ku, Yokohama-shi, Kanagawa 230-0045, Japan

[¶]Mechanical and Aerospace Engineering Department, University of California, Los Angeles, 420 Westwood Plaza, Los Angeles, California 90095-1597

This paper presents an inverse method for retrieving (i) the true thermal conductivity, and (ii) the two-band absorption coefficient of soda-lime silicate glassmelts between 1100°C and 1550°C from measured steady-state temperature profiles. This was achieved by combining (i) a forward method solving combined conductive and radiative heat transfer accounting for temperature-dependent thermal conductivity and spectral absorption coefficient and (ii) an inverse method based on genetic algorithm (GA) optimization. Four glassmelt compositions from ultraclear to gray glasses with iron content ranging from 0.008 to 1.1 wt% were investigated. First, it was established that the steady-state temperature in glassmelt can be predicted accurately by averaging the spectral absorption coefficient over two bands from 0 to 2.8 μm and 2.8 to 5.0 μm. The inverse method showed that the true thermal conductivity was independent of the iron content and given by $k_c(T) = 1.31 + 5.90 \times 10^{-4}T$, where T is given in °C. In addition, the band absorption coefficient between 0 and 2.8 μm strongly increased with increasing iron content, while the band absorption coefficient between 2.8–5.0 μm was independent of iron content.

I. Introduction

Soda-lime silicate glass is used in numerous applications. For example, clear and tinted glasses are used for building windows while so-called "solar control glass" is used for automotive windows.[1] The latter, characterized by a light green tint, contains relatively large iron content around 1.0 wt% to absorb harmful ultraviolet (UV) and infrared solar radiation. In addition, clear soda-lime silicate glasses, featuring very low iron content and high transmittance, have been used as substrate in solar cells.[2,3]

Knowing the temperature distribution and temperature history of the glassmelt is essential in the manufacturing process of the above-mentioned glass products. It enables proper control of the production and ensures quality of the final products.[4] Heat transfer in semitransparent glassmelts at high temperatures is strongly affected by radiation heat transfer. Glassmelts with high iron content, such as gray and green soda-lime silicate glasses, strongly absorb thermal radiation.[5] Then, radiation transfer can be treated as a diffusion process [5–7] and the local heat flux is given by Fourier's law with an effective thermal conductivity defined as the sum of the true (or phononic) thermal conductivity and the radiative thermal conductivity based on Rosseland diffusion approximation.[8] However, for glassmelts with low iron content, featuring low absorption coefficient, thermal radiation transfer can no longer be regarded as a diffusion process. Then, in order to predict the temperature distribution in such glassmelts, the true thermal conductivity, the absorption coefficient of the glassmelts, and the emissivity of the boundaries are required.

This study presents an inverse method to retrieve (i) the true thermal conductivity, and (ii) the absorption coefficient of soda-lime silicate glassmelts from experimentally measured temperature profiles at temperatures between 1100°C and 1550°C. The method was applied to four types of soda-lime silicate glassmelts with iron content ranging from 0.008 to 1.1 wt%.

II. Background

(1) Combined Conductive and Radiative Heat Transfer

In semitransparent glassmelts, heat is transferred by both conduction and radiation. To predict the local temperature $T(\hat{r}, t)$, one needs to solve the energy conservation equation expressed as[8,9]

$$\rho(T)c_p(T)\frac{\partial T}{\partial t} = \nabla \cdot (k_c(T)\nabla T) - \nabla \cdot \vec{q}_r \tag{1}$$

Here, the divergence of the radiative heat flux $\vec{q}_r$ is defined as [8,9]

$$\nabla \cdot \vec{q}_r = \int_0^\infty \left[4\pi n_\lambda^2 I_{b,\lambda}(T(\hat{r}, t)) - G_\lambda(\hat{r})\right] d\lambda \tag{2}$$

where $I_{b,\lambda}(T(\hat{r}, t))$ is the local spectral blackbody radiation intensity, G_λ is the spectral fluence rate defined as $G_\lambda(\hat{r}) = \int_{4\pi} I_\lambda(\hat{s}, \hat{r}) d\Omega$. The spectral intensity $I_\lambda(\hat{s}, \hat{r})$ at location $\hat{r}$ in direction $\hat{s}$ is governed by the radiative transfer equation (RTE). For an absorbing and emitting, but nonscattering media, the RTE can be written as[8,9]

$$\hat{s} \cdot \nabla I_\lambda = -\kappa_\lambda I_\lambda + \kappa_\lambda n_\lambda^2 I_{b,\lambda}(T(\hat{r}, t)) \tag{3}$$

where $\kappa_\lambda = 4\pi k_\lambda/\lambda$ is the spectral absorption coefficient, while n_λ and k_λ are the real and imaginary parts of the

J. Mauro—contributing editor

Manuscript No. 37427. Received August 28, 2015; approved November 30, 2015.
[†]Author to whom correspondence should be addressed. e.mail: pilon@seas.ucla.edu

complex index of refraction m_λ of the glassmelt defined as $m_\lambda = n_\lambda - ik_\lambda$.

(2) Rosseland Diffusion Approximation

In the limiting case of optically thick glassmelts, the photon mean free path is much smaller than the characteristic length of the medium. Then, radiation can be treated as a diffusion process based on the Rosseland diffusion approximation. The total heat flux $\vec{q}_{\text{total}}$ can be expressed as the sum of the conductive $\vec{q}_{\text{c}}$ and radiative $\vec{q}_{\text{r}}$ heat fluxes both given by Fourier's law as [8]

$$\vec{q}_{\text{total}} = \vec{q}_{\text{c}} + \vec{q}_{\text{r}} = -k_{\text{c}}(T)\nabla T - k_{\text{r}}(T)\nabla T = -k_{\text{eff}}(T)\nabla T \tag{4}$$

where $k_{\text{c}}(T)$ and $k_{\text{r}}(T)$ are the conductive (or true) and radiative thermal conductivities, respectively. The effective thermal conductivity k_{eff} (T) can be expressed as the sum of the true and radiative thermal conductivities [8]

$$k_{\text{eff}}(T) = k_{\text{c}}(T) + k_{\text{r}}(T) \tag{5}$$

Based on the Rosseland diffusion approximation, the radiative thermal conductivity $k_{\text{r}}(T)$ can be expressed as[8,9]

$$k_{\text{r}}(T) = \frac{16n^2\sigma T^3}{3\kappa_{\text{R}}} \tag{6}$$

where σ is the Stefan–Boltzmann constant ($\sigma = 5.67 \times 10^{-8}$ W/m^{2}K^4). The Rosseland mean absorption coefficient κ_{R} can be computed from the spectral absorption coefficient κ_λ and the refractive index n_λ of the glassmelt according to[8]

$$\frac{n^2}{\kappa_{\text{R}}} = \frac{\pi}{4\sigma T^3}\int_0^\infty \frac{n_\lambda^2}{\kappa_\lambda}\frac{\mathrm{d}I_{\text{b},\lambda}(T)}{\mathrm{d}T}\mathrm{d}\lambda \tag{7}$$

where the blackbody spectral intensity $I_{\text{b},\lambda}(T)$ under vacuum is given by Planck's law, and its derivative with respect to temperature T in K is expressed as [8,9]

$$\frac{\mathrm{d}I_{\text{b},\lambda}(T)}{\mathrm{d}T} = \frac{2hc^2}{\lambda^6 k_{\text{B}} T^2}\frac{\exp(hc/\lambda k_{\text{B}}T)}{[\exp(hc/\lambda k_{\text{B}}T) - 1]^2} \tag{8}$$

Here, h, c, and k_{B} are the Planck's constant ($h = 6.626068 \times 10^{-34}$ m^{2}kg/s), the speed of light under vacuum ($c = 299\,792\,458$ m/s), and the Boltzmann constant ($k_{\text{B}} = 1.3806503 \times 10^{-23}$ m^{2}kgs^{-2}K^{-1}), respectively.

(3) Experiment

Experimental methods to measure the effective thermal conductivity $k_{\text{eff}}(T)$ of glassmelt at high temperature have been reviewed in Ref. [10] and need not be repeated. In brief, they can be divided into steady-state and transient methods.[11,12] Steady-state methods such as the linear heat flow method,[10,13] the radial heat flow method,[11] and the interferometric method,[7] measure directly the effective thermal conductivity of glassmelts including both conductive and radiative contributions. Transient methods include the laser flash method,[14,15] the hot wire method,[16] the periodic heat flow method,[17] and the needle probe method.[18] These transient methods have been used to determine the effective thermal diffusivity of glassmelt and retrieve the effective thermal conductivity based on the glassmelt's density and specific heat.

Endrys and Turzik[19] measured the effective thermal conductivity of solid glass samples. They obtained the true thermal conductivity $k_{\text{c}}(T)$ by subtracting the radiative thermal conductivity $k_{\text{r}}(T)$ predicted by Rosseland diffusion approximation using the spectral absorption coefficient and the refractive index of the glass samples. André and Degiovanni[20] developed a combined conductive and radiative heat transfer model for the transient flash method. They proved that the flash method can measure the true thermal diffusivity of semitransparent materials if the sample features reflecting surfaces (e.g., gold coated) and an equivalent optical thickness less than 0.1 based on the Rosseland or Planck mean absorption coefficient. The authors measured the true thermal diffusivity of solid float glass, featuring 0.09 wt% of Fe_2O_3 and coated with gold, between 25°C and 500°C. Lazard et al.[21] retrieved the true thermal conductivity of solid float glass between 20°C and 427°C using the laser flash method and rear-face thermograms. The glass samples were assumed to be gray, and a semianalytical model was employed to account for combined conduction and radiation. The optimization was implemented using the Levenberg–Marquardt algorithm to retrieve the glass optical thickness, Planck number, phononic diffusivity, and Biot number. Unfortunately, the authors did not report the iron content and the thickness of the float glass samples investigated. Mann et al.[22] experimentally determined the true thermal conductivity of solid soda-lime float glass between 240°C and 500°C. A plane-parallel glass slab was heated to a uniform initial temperature near the softening point. It was then immediately transferred to the laboratory ambient, and the time-dependent boundary and center-plane temperatures were recorded as the sample cooled down, using embedded thermocouples. The temperatures measured at the sample surfaces were used as boundary conditions of a combined conductive and radiative heat transfer model. The volumetric heat capacity ρc_{p} was measured independently, while the spectral absorption coefficient κ_λ was taken from the literature.[23] The temperature-dependent true thermal conductivity $k_{\text{c}}(T)$ was obtained by matching the experimentally measured time-dependent center-plane temperature with those predicted theoretically. It was found to be $k_{\text{c}}(T) = 1.14 + 6.24 \times 10^{-4}T$, with T given in °C. Although the authors did not report the iron content of the float glass investigated, this formula has been used for various soda-lime silicate glasses with different iron contents.[24,25]

Unlike previous studies, the present effort considered molten glass samples with known iron content and retrieved simultaneously their true thermal conductivity and the spectral absorption coefficient from actual steady-state temperature measurements. The inverse method developed used genetic algorithm (GA) [26,27] as the optimization method and a numerical solver for Eqs. (1–3) based on finite volume and Monte Carlo method (MCM) for the forward problem. Finally, the validity of the Rosseland diffusion approximation was systematically discussed.

III. Analysis

(1) Schematic and Assumptions

The four types of soda-lime silicate glassmelts investigated in this paper along with the experimental setup measuring the steady-state temperature profile for different furnace temperature T_{f} have been described in detail in Ref. [10]. The uncertainties for the measured temperatures were estimated to be $\Delta T = 5$°C as discussed in our previous study.[10] Soda-lime silicate glass with the prescribed composition was crushed and melted in a high-alumina crucible of large cross section and heated from the top in a high-temperature furnace. The thickness L of the glassmelt varied between 14 and 17 cm depending on the glassmelts composition. The steady-state temperature profile was measured by inserting a type-B sheathed thermocouple into the glassmelt along the center line of the crucible. The furnace temperature T_{f} varied from 1300°C to 1500°C or 1550°C by 50°C increment.

Figure 1 shows schematically the experimental apparatus along with the coordinate system and the different variables considered. To simplify the problem, the following assumptions were made:

1. One dimensional (1D) heat transfer prevailed along the x-direction. This was valid by virtue of the fact that (1) the thickness of the glassmelt was small compared with the cross section of the crucible, (2) the temperature distribution was measured along the crucible center line, thus minimizing edge effects, (3) the effective thermal conductivity of the glassmelt considered was 4 to 40 times larger than that of the crucible, (4) the furnace crown served as a reradiating surface, thus ensuring the incident radiation was diffuse and uniform over the glassmelt surface.
2. The glassmelts were considered to be opaque for wavelengths larger than $\lambda_{cut} = 5.0$ μm as established in the literatures.[22,24,25] Indeed, beyond $\lambda_{cut} = 5.0$ μm, κ_λ exceed 5×10^3 m^{-1} and the photon mean free path was less than 0.2 mm for all glass compositions considered.[24] In fact, the effect of λ_{cut} on the steady-state temperature profiles was found to be negligible for λ_{cut} between 5.0 and 8.0 μm (see Fig. S1 in Supplementary Materials).
3. The top surface ($x = L$) of the glassmelt was treated as optically smooth, semitransparent, and specularly reflecting. The spectral directional reflectivity $\rho_{L,\lambda}(\theta)$ of the surface was calculated by combining Fresnel's equations for reflection and Snell's law of refraction.[8,9] The emissivity in the opaque spectral region ($\lambda > \lambda_{cut}$) at the glassmelt surface located at $x = L$ was taken as $\varepsilon_L = 0.9$, as reported in Ref. [24].
4. The alumina crucible was assumed to be opaque, gray, and diffusely reflecting and emitting with emissivity ε_0 taken as $\varepsilon_0 = 1.0$ by analogy with Ref. [24, 25, 28]. In fact, the normal spectral emissivity of the crucible in the glassmelt can be estimated by[8]

$$\varepsilon_{0,\lambda,n} = 1 - \rho_{\lambda,n} = 1 - \frac{\left(n_{\lambda,2} - n_{\lambda,1}\right)^2 + \left(k_{\lambda,2} - k_{\lambda,1}\right)^2}{\left(n_{\lambda,2} + n_{\lambda,1}\right)^2 + \left(k_{\lambda,2} + k_{\lambda,1}\right)^2} \tag{9}$$

Here, $\rho_{\lambda,n}$ is the spectral normal reflectivity of the crucible wall in the glassmelt while $n_{\lambda,1}$, $k_{\lambda,1}$ and $n_{\lambda,2}$, $k_{\lambda,2}$ are the refractive and absorption indices of the glassmelt and crucible, respectively. The refractive and absorption indices of alumina was reported in Ref. [29] while that of gray, green, bronze, clear, and low-iron soda-lime silicate glasses at room temperature was reported by Rubin.[23] Then, the estimated normal emissivity $\varepsilon_{0,\lambda,n}$ of the crucible wall was larger than 0.99 for the different glassmelt compositions and over the spectral region from 0 to λ_{cut} (see Fig. S2 in Supplementary Materials).

5. The refractive index of the glass was considered to be constant, independent of temperature, and equal to $n_\lambda = 1.49$ over the spectral region 0–5.0 μm, as assumed in Ref. [24].
6. The true glassmelt thermal conductivity was assumed to be linearly dependent on temperature so that $k_c(T) = a + bT$, where T is expressed in °C.[22]
7. The spectral absorption coefficient of the glassmelt was assumed to be constant over two spectral bands, i.e., $\kappa_\lambda = \kappa_1$ for λ between 0 and 2.8 μm and $\kappa_\lambda = \kappa_2$ for λ ranging from 2.8–5.0 μm as suggested by the optical properties of different soda-lime silicate glasses.[23]

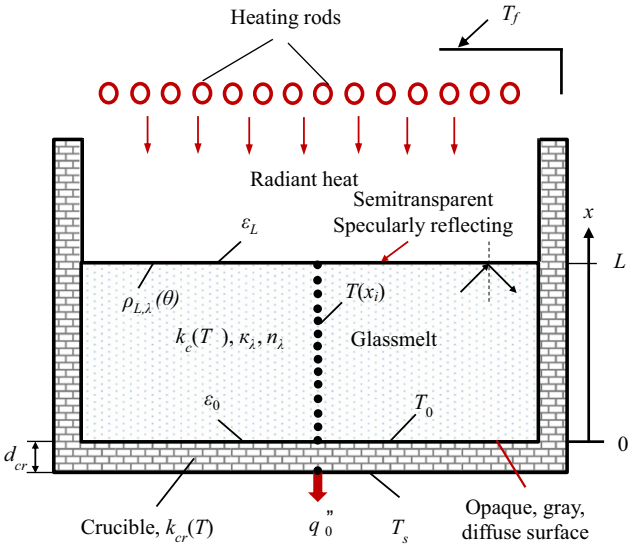

Fig. 1. Schematic of the physical model and of the associated coordinate system.

(2) Governing equations and boundary conditions

The 1D temperature profile in the glassmelt can be predicted by solving Eqs. (1–3). The boundary condition at the bottom of the glassmelt in contact with the crucible located at $x = 0$ can be written as[24]

$$-k_c(T)\frac{dT}{dx}(0) - \alpha_0 \int_0^{\lambda_{cut}} q''_{r,\lambda}(0)d\lambda + \pi\varepsilon_0 \int_0^{\lambda_{cut}} I_{b\lambda}[T(0)]d\lambda = q''_0 \tag{10}$$

where α_0 and ε_0 are the total hemispherical absorptivity and emissivity of the crucible bottom in contact with the glassmelt, $q''_{r,\lambda}$ is the spectral radiation heat flux. Here, q''_0 is the conductive heat flux measured across the crucible bottom wall, and given by $q''_0 = -k_{cr}[T(x=0) - T_S]/d_{cr}$, where k_{cr} and d_{cr} are the thermal conductivity and thickness of the crucible and T_S is the temperature at the outer surface of the crucible's bottom (Fig. 1).

The boundary condition at the top of the glassmelt located at $x = L$ can be written as[24]

$$-k_c(T)\frac{dT}{dx}(L) = \pi\varepsilon_L\left\{\int_{\lambda_{cut}}^{\infty} I_{b\lambda}[T(L)]d\lambda - \int_{\lambda_{cut}}^{\infty} I_{b\lambda}(T_f)d\lambda\right\} \tag{11}$$

where ε_L is the total hemispherical emissivity of surface $x = L$ for the spectral range where the glassmelt is considered to be opaque to thermal radiation.

The MCM was employed to solve the RTE on a spectral basis while the finite volume method was used to solve the energy equation. The steady-state solution was considered to be reached when the relative difference in local temperature $T(x)$ between two consecutive time steps did not exceed 10^{-6}.

(3) Verification of the Combined Heat Transfer Model

In order to validate the combined conduction and radiation computer program used in the forward problem, we compared the predicted steady-state temperature profile with that reported by Lee and Viskanta[24] for a plane-parallel slab of float and green glasses. The top of the glass slab was a free surface assumed to be optically smooth and specularly

reflecting, like in this study. The authors used the spectral absorption coefficient of clear and green soda-lime silicate glasses reported by Rubin.[23] The spectrum was decomposed in eight spectral bands (see Fig. S3 in Supplementary Materials). The true thermal conductivity for float and green glass was taken as $k_c(T) = 1.14 + 6.24 \times 10^{-4}T$, where T is given in °C.[22] Temperature profiles predicted by the present code were in good agreement with those reported by Lee and Viskanta[24] for both types of glass and for three different slab thicknesses L of 0.01, 0.1, and 1.0 m (see Fig. S4 in Supplementary Materials).

(4) Verification of Two-Band Approximation for Glassmelts

In order to simplify the inverse method, the spectral absorption coefficient of soda-lime silicate glasses was approximated as constant over two spectral bands below 5.0 μm, i.e., $\kappa_\lambda = \kappa_1$ for λ between 0 and 2.8 μm and $\kappa_\lambda = \kappa_2$ for λ in the band 2.8–5.0 μm.[23] To validate this assumption, let us consider a slab of high-iron (gray) and low-iron content soda-lime silicate glassmelts (see Fig. S5 in Supplementary Materials). The true thermal conductivity of both glasses was taken as $k_c(T) = 1.14 + 6.24 \times 10^{-4}T$.[22] The furnace temperature T_f was set as 1400°C, while the thickness L was 14 cm for the gray glassmelt and 16 cm for the low-iron glassmelt. Two-band Rosseland mean absorption coefficients $\kappa_{R,1}$ and $\kappa_{R,2}$ can be defined for each band $[\lambda_{i,\min}, \lambda_{i,\max}]$ taken as $[0, \lambda_1]$ for $i = 1$ and as $[\lambda_1, \lambda_{cut}]$ for $i = 2$ as

$$\frac{1}{\kappa_{R,i}} = \int_{\lambda_{i,\min}}^{\lambda_{i,\max}} \frac{1}{\kappa_\lambda}\frac{dI_{b,\lambda}(T)}{dT}d\lambda \Big/ \int_{\lambda_{i,\min}}^{\lambda_{i,\max}} \frac{dI_{b,\lambda}(T)}{dT}d\lambda \tag{12}$$

Here, the wavelength $\lambda_1 = 2.8$ μm and $\lambda_{cut} = 5.0$ μm, the temperature T used in Eq. (12) was 1355°C and 1380°C for gray and low-iron glassmelts, respectively. These values corresponded to the average glassmelt temperature predicted using the spectral absorption coefficient reported by Rubin.[23] Here, the total hemispherical emissivity ε_0 was taken as unity. The total heat flux q_0'' across the gray and low-iron glassmelts was taken arbitrarily as 12 000 and 15 000 W/m^2, respectively. For the gray glassmelt, the maximum difference in the temperature profiles predicted using (i) the spectral absorption coefficient[23] and (ii) the two-band approximation was about 8°C or 0.6%. For the low-iron glassmelt, the temperature difference was less than 4°C or 0.3% (see Fig. S6 in Supplementary Materials). These results indicate that the two-band model gives acceptable results and can be used to predict the steady-state temperature profile in soda-lime silicate glassmelts for both low and high iron contents.

(5) Inverse Method

The goal of the inverse problem was to retrieve (i) the true thermal conductivity $k_c(T) = a + bT$, where a and b are unknown parameters and (ii) the band absorption coefficients κ_1 and κ_2 in the spectral bands 0–2.8 μm and 2.8–5.0 μm, respectively. In addition, the furnace temperature T_f was not measured accurately in the experiments described in Ref. [10]. However, the predicted temperature profile was very sensitive to T_f as it directly affected the boundary condition at surface $x = L$ [Eq. (11)]. Therefore, the furnace temperature was also regarded as an unknown parameter to be retrieved and denoted by $T_{f,R}$. Overall, five parameters were retrieved from the experimentally measured temperature profile, namely a, b, κ_1, κ_2, and $T_{f,R}$. This was achieved by minimizing the fitness function F defined as

$$F = \frac{1}{N}\left[\sum_{i=1}^{N}\sqrt{\left(\frac{T_{exp}(x_i) - T_{pred}(x_i)}{T_{exp}(x_i)}\right)^2}\right] \tag{13}$$

where $T_{exp}(x_i)$ and $T_{pred}(x_i)$ are the experimentally measured and numerically predicted temperatures at N discrete depths x_i in the glassmelt.

Figure 2 shows the block diagram of the inverse method based on genetic algorithm (GA) and used to minimize the fitness function F. The input parameters included the glassmelt depth L, the total heat flux q_0'', the glassmelt refractive index n, its emissivities ε_0 and ε_L at the bottom and top surfaces. The GA optimization was such that the minimum and maximum number of generations was 20 and 70 while the number of individuals P per generation was 100. First, P individual sets of parameters (a, b, κ_1, κ_2, $T_{f,R}$) were generated randomly. The bounds for parameters a, b, κ_2, and $T_{f,R}$ for all glassmelts were such that $a \in [1.0, 2.0]$ W·(m·K)$^{-1}$, $b \in [10^{-4}, 10^{-3}]$ W·(m·K)$^{-1}$, $\kappa_2 \in [300, 600]$ m^{-1}, and $T_{f,R} \in [T_f - 50, T_f + 50]$ °C, respectively. The bound for parameter κ_1 was set as $\kappa_1 \in [100, 300]$ m^{-1} for gray and green glassmelts while it was $\kappa_1 \in [0, 80]$ m^{-1} for clear and low-iron glassmelts based on data reported by Rubin.[23] Then, the corresponding temperature profiles were computed by numerically solving Eqs. (1–3), (10) and (11). The fitness function F was computed for each individual. The convergence criteria was satisfied if the fitness function of the best individual was smaller than the tolerance error of 10^{-3}. In the event when the fitness function of the best individual was larger than 10^{-3} after 50 generations, 20 additional generations were performed, and the best individual with the lowest fitness function was retained. In all cases, the fitness function was less than 3×10^{-3}, which was considered acceptable.

The inverse method was successfully validated by retrieving the input parameters from numerically generated temperature profiles predicted from the combined conduction and radiation model using realistic values of the parameters a, b, κ_1, κ_2, and $T_{f,R}$. In all cases, the inverse method was able to retrieve the imposed values of $k_c(T)$, κ_1, κ_2, and $T_{f,R}$ within about 10% (see Table S1 in Supplementary Materials).

IV. Results and Discussion

(1) Composition 1: Gray Soda-Lime Silicate Glassmelt

Table I reports the values of parameters a, b, κ_1, κ_2, and $T_{f,R}$ retrieved by the inverse method for gray soda-lime silicate glassmelt with 1.1 wt% Fe_2O_3 (composition 1) for furnace temperature T_f of 1300°C, 1350°C, 1400°C, 1450°C, 1500°C,

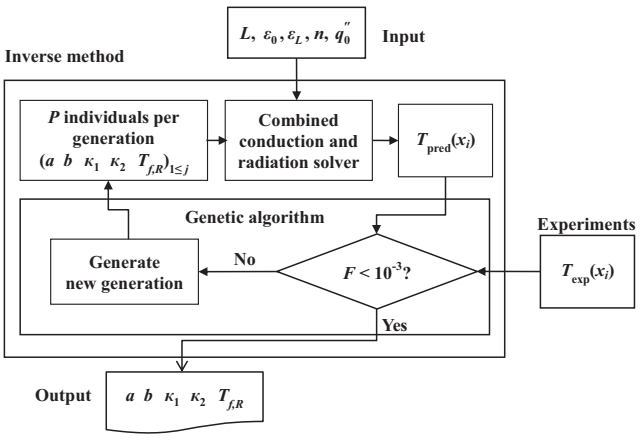

Fig. 2. Block diagram of the inverse method used in this study to retrieve the parameters (a, b, κ_1, κ_2, $T_{f,R}$) from the experimental temperature profile $T_{exp}(x_i)$.

Table I. Retrieved Parameters for Gray Soda-Lime Glassmelt (composition 1) for Furnace Temperature T_f Between 1300°C and 1550°C

	Retrieved parameters					
Set furnace temperature T_f (°C)	$T_{f,R}$ (°C)	a (W/m·K)	b (W/m·K^2)	κ_1 (m^{-1})	κ_2 (m^{-1})	Fitness, F
1300	1296	1.05	6.50×10^{-4}	219.2	445.8	1.03×10^{-3}
1350	1348	1.75	2.60×10^{-4}	215.6	452.6	1.00×10^{-3}
1400	1396	1.14	6.35×10^{-4}	212.0	402.0	8.98×10^{-4}
1450	1451	1.30	6.27×10^{-4}	234.8	473.0	1.29×10^{-3}
1500	1503	1.51	4.39×10^{-4}	212.1	433.0	9.00×10^{-4}
1550	1552	1.84	1.15×10^{-4}	214.0	447.6	3.14×10^{-4}

and 1550°C. First, it is interesting to note that the retrieved furnace temperature $T_{f,R}$ fell within 4°C of its set value. In addition, the fitness function approached or was below 10^{-3}. The retrieved values of a and b were less consistent. However, this should be assessed only by considering the retrieved true thermal conductivity $k_c(T) = a + bT$. In fact, Fig. 3(a) shows the true thermal conductivity $k_c(T)$ retrieved for gray soda-lime silicate glassmelt. It indicates that $k_c(T)$ was consistent from one furnace temperature to another. It increased from about 1.9 to 2.2 W·(m·K)$^{-1}$ as the temperature of the glassmelt increased from 1140°C to 1550°C. More importantly, the retrieved values of $k_c(T)$ agreed very well with that reported by Mann et al.[22] for solid soda-lime silicate glass at temperature between 240°C and 500°C. In addition, Fig. 3(a) shows the effective thermal conductivity $k_{eff}(T)$ predicted by Eqs. (5–8) using the two-band absorption coefficient approximation. It also reproduces the predictions of the expression of $k_{eff}(T)$ reported in Ref. [10] and obtained by treating radiation as a diffusion process. The results for $k_{eff}(T)$ retrieved in this study fell within 10% of those reported in Ref. [10].

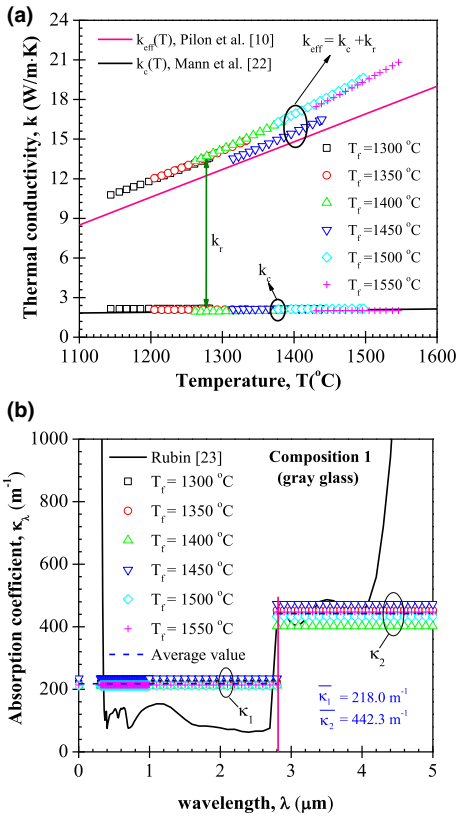

Fig. 3. Retrieved (a) true and effective thermal conductivities and (b) absorption coefficient of gray soda-lime silicate glassmelt (composition 1) for furnace temperature between 1300°C and 1550°C. Also shown are (i) the prediction of $k_c(T)$ from Ref. [22] (ii) the prediction of $k_{eff}(T)$ for gray glass from Ref. [10], and (iii) the experimental data of κ_λ for gray glass from Ref. [23].

Figure 3(b) shows the two-band absorption coefficients κ_1 and κ_2 retrieved for the gray soda-lime silicate glassmelt in the spectral bands 0–2.8 μm and 2.8–5.0 μm for different furnace temperatures. It indicates that the retrieved values of κ_1 and κ_2 were consistent from one furnace temperature to another. Their average values were $\overline{\kappa}_1 = 218.0$ m^{-1} and $\overline{\kappa}_2 = 442.3$ m^{-1}, respectively. Figure 3(b) also shows the spectral absorption coefficient of "gray" soda-lime silicate glass, reported by Rubin,[23] but of unknown iron content. It is evident that the retrieved value of $\overline{\kappa}_1$ was larger than that reported by Rubin.[23] On the other hand, $\overline{\kappa}_2$ agreed well with Rubin's data in the 2.8–5.0 μm band. This may due to the fact that the iron content was different between these two "gray" glasses. Indeed, the iron content strongly affected the spectral absorption of glass coefficient between 0 and 2.8 μm and significantly less between 2.8 and 5.0 μm as discussed in the next sections.

Figure 4 compares the experimentally measured temperature profiles with that numerically predicted by accounting for combined conduction and radiation using the retrieved parameters shown in Table I for set furnace temperature T_f of 1300°C and 1550°C. It indicates that the numerically predicted temperature profiles fell within the experimental uncertainty. Similar results and conclusions were obtained for the other furnace temperatures (see Fig. S7 in Supplementary Materials).

(2) Composition 2: Green Soda-Lime Silicate Glassmelt

Table II reports the values of a, b, κ_1, κ_2, and $T_{f,R}$ retrieved for green soda-lime silicate glassmelt with 0.512% Fe_2O_3 (composition 2) for furnace temperature T_f between 1300°C and 1500°C. The retrieved temperature $T_{f,R}$ followed the same trend as T_f, but was systematically lower by 20°C–35°C corresponding to a relative difference of less than 3%.

Figure 5(a) shows the retrieved true thermal conductivity $k_c(T)$ for green soda-lime silicate glassmelt. Here also, the retrieved values of $k_c(T)$ were consistent and agreed well with

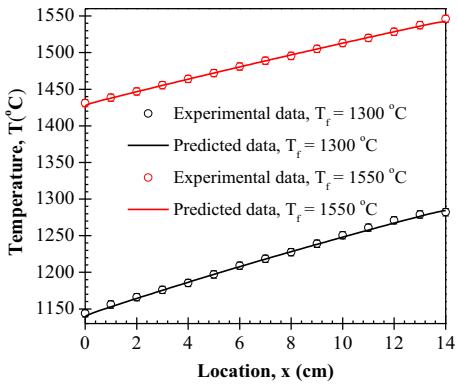

Fig. 4. Comparison between experimentally measured and numerically predicted temperature profiles using the retrieved properties reported in Table I for gray soda-lime silicate glassmelt (composition 1) at furnace temperature T_f of 1300°C and 1550°C.

Table II. Retrieved Parameters for Green Soda-Lime Glassmelt (composition 2) for Furnace Temperature T_f Between 1300°C and 1500°C

	Retrieved parameters					
Set furnace temperature T_f (°C)	$T_{f,R}$ (°C)	a (W/m·K)	b (W/m·K^2)	κ_1 (m^{-1})	κ_2 (m^{-1})	Fitness, F
1300	1267	1.47	4.77×10^{-4}	165.8	410.0	2.10×10^{-3}
1350	1317	1.61	3.80×10^{-4}	183.7	493.5	2.17×10^{-3}
1400	1375	1.60	4.18×10^{-4}	183.7	403.8	1.66×10^{-3}
1450	1424	1.16	6.32×10^{-4}	177.8	495.9	1.44×10^{-3}
1500	1477	1.52	3.90×10^{-4}	182.6	486.9	3.40×10^{-4}

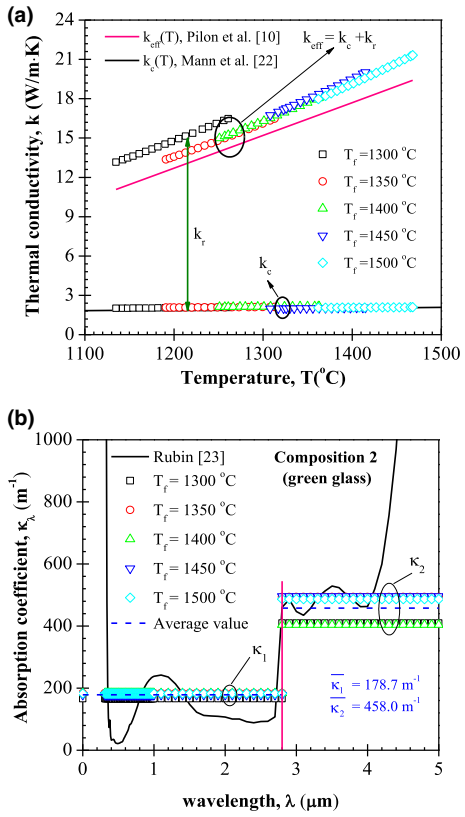

Fig. 5. Retrieved (a) true and effective thermal conductivities and (b) absorption coefficient of green soda-lime silicate glassmelt (composition 2) for furnace temperature between 1300°C and 1500°C. Also shown are (i) the prediction of $k_c(T)$ from Ref. [22] (ii) the prediction of $k_{eff}(T)$ for green glass from Ref. [10], and (iii) the experimental data of κ_λ for green glass from Ref. [23].

the expression reported by Mann et al.[22] Figure 5(a) also shows the effective thermal conductivity $k_{eff}(T)$ predicted by Eqs. (5–8) using the two-band absorption coefficient approximation along with the expression of $k_{eff}(T)$ reported in Ref. [10] and obtained by treating radiation as a diffusion process. Here also, the estimates of $k_{eff}(T)$ fell within 10% of those reported in Ref. [10]. Based on the retrieved two-band absorption coefficient, the spectrally averaged mean free path of photons in gray and green glassmelts between 1100°C and 1500°C, estimated as $l_R = 1/\kappa_R$, was about 0.45 and 0.55 cm, respectively. These values were much smaller than the glassmelt thickness of 14 and 17 cm, so that the gray and the green glassmelts can be treated as optically thick and radiation transfer as a diffusion process.

Figure 5(b) shows the two-band absorption coefficients κ_1 and κ_2 of the green soda-lime silicate glassmelt in the spectral ranges 0–2.8 μm and 2.8–5.0 μm retrieved for different furnace temperatures for the green soda-lime silicate glassmelt. It indicates that the retrieved values of κ_1 and κ_2 were consistent for different furnace temperatures. Their average values $\overline{\kappa}_1$ and $\overline{\kappa}_2$ were equal to 178.7 and 458.0 m^{-1}, respectively. In other words, a reduction in iron content from 1.1 to 0.512 wt% resulted in a relatively small (~18%) decrease in absorption coefficient $\overline{\kappa}_1$ of the soda-lime silicate glassmelt, while the absorption coefficient $\overline{\kappa}_2$ remained almost unchanged. In addition, Fig. 5(b) plots the spectral absorption coefficient of green glass reported by Rubin.[23] It shows that the retrieved values of κ_1 and κ_2 agreed well with Rubin's data for both spectral bands 0–2.8 μm and 2.8–5.0 μm. Finally, the numerically predicted temperature profiles for green glassmelt using the retrieved parameters shown in Table II for all furnace temperatures were also in good agreement with experimental data (see Fig. S8 in Supplementary Materials).

(3) Composition 3: Clear Soda-Lime Silicate Glassmelt

Table III reports the values of a, b, κ_1, κ_2, and $T_{f,R}$ retrieved for clear soda-lime silicate glassmelt with 0.084 wt% Fe_2O_3 (composition 3) for furnace temperature T_f between 1300°C and 1500°C. Here also, the retrieved furnace temperature $T_{f,R}$ followed the same trend as the set value, but was systematically lower by 20°C–40°C, i.e., by less than 3%.

Figure 6(a) shows the retrieved true thermal conductivity $k_c(T)$ for clear soda-lime silicate glassmelt. It indicates that $k_c(T)$ increased from about 1.8 to 2.5 W·(m·K)$^{-1}$ as the glassmelt temperature increased from 1200°C to 1480°C. It agreed well with the expression reported by Mann et al.[22] Figure 6(a) also shows the effective thermal conductivity $k_{eff}(T)$ predicted by Eqs. (5–8) using the two-band absorption coefficient (κ_1,κ_2). It deviated significantly from those reported in Ref. [10].

Table III. Retrieved Parameters for Clear Soda-Lime Glassmelt (composition 3) for Furnace Temperature T_f Between 1300°C and 1500°C

	Retrieved parameters					
Set furnace temperature T_f (°C)	$T_{f,R}$ (°C)	a (W/m·K)	b (W/m·K^2)	κ_1 (m^{-1})	κ_2 (m^{-1})	Fitness, F
1300	1261	1.40	4.66×10^{-4}	39.3	456.9	6.25×10^{-4}
1350	1317	1.65	4.95×10^{-4}	42.5	472.4	6.77×10^{-4}
1400	1373	1.01	5.89×10^{-4}	41.0	459.0	5.19×10^{-4}
1450	1426	1.21	5.72×10^{-4}	49.8	453.7	8.28×10^{-4}
1500	1476	1.65	5.84×10^{-4}	41.4	453.8	1.19×10^{-3}

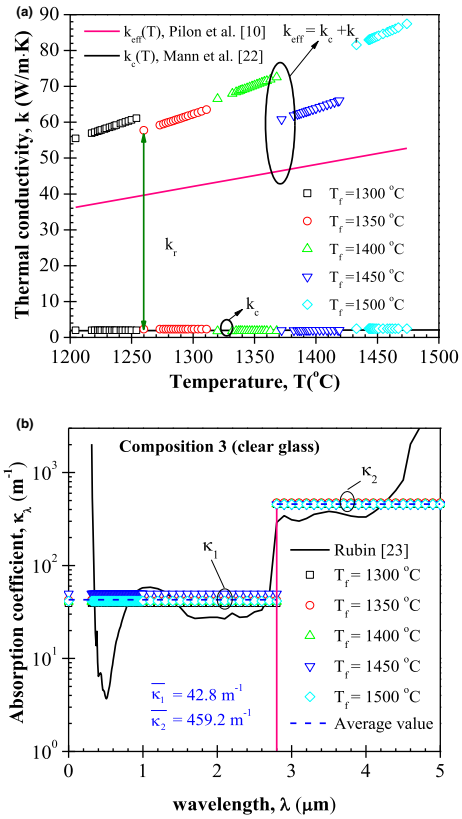

Fig. 6. Retrieved (a) true and effective thermal conductivities and (b) absorption coefficient of clear soda-lime silicate glassmelt (composition 3) for furnace temperature between 1300°C and 1500°C. Also shown are (i) the prediction of $k_c(T)$ from Ref. [22] (ii) the prediction of $k_{eff}(T)$ for clear glass from Ref. [10], and (iii) the experimental data of κ_λ for clear glass from Ref. [23].

Figure 6(b) shows the two-band absorption coefficients κ_1 and κ_2 in the spectral bands 0–2.8 μm and 2.8–5.0 μm retrieved for different furnace temperatures as well as the spectral absorption coefficient κ_λ reported by Rubin[23] for clear soda-lime silicate glass of unknown iron content. It indicates that the retrieved values of κ_1 and κ_2 for different furnace temperatures were consistent from one set furnace temperature to another with average values of $\overline{\kappa}_1 = 42.8$ m^{-1} and $\overline{\kappa}_2 = 459.2$ m^{-1}. The average absorption coefficient $\overline{\kappa}_1$ decreased from 218.0 m^{-1} to 178.7 m^{-1} and 42.8 m^{-1} as the iron content decreased from 1.1 wt% to 0.512 wt% and 0.084 wt.%. On the other hand, the average band absorption coefficient κ_2 remained almost unchanged. Finally, the numerically predicted temperature profiles obtained using the retrieved parameters shown in Table III for all furnace temperatures were in good agreement with experimental measurements (see Fig. S9 in Supplementary Materials).

(4) Composition 4: Low-Iron Soda-Lime Silicate Glassmelt

Table IV reports the values of a, b, κ_1, κ_2, and $T_{f,R}$ retrieved for low-iron (ultraclear) soda-lime silicate glassmelt with 0.008 wt% Fe_2O_3 (composition 4) for furnace temperature T_f between 1300°C and 1500°C. The retrieved furnace temperature $T_{f,R}$ followed the same trend as the set value, but was systematically lower by 10°C–15°C, or less than 2%.

Figure 7(a) shows the retrieved true thermal conductivity $k_c(T)$ for low-iron soda-lime silicate glassmelt. It indicates that, here also, the true thermal conductivity $k_c(T)$ was in good agreement with that reported by Mann et al.[22] In addition, Fig. 7(a) shows the effective thermal conductivity $k_{eff}(T)$ predicted from Eqs. (5–8) using the true thermal conductivity $k_c(T)$ and the two-band absorption coefficient approximation. It is obvious that predictions of $k_{eff}(T)$ were significantly larger than those reported in Ref. [10] This was due to the fact that the absorption coefficient for clear and low iron soda-lime silicate glassmelts was relatively small. In fact, the corresponding averaged photon mean free paths were, respectively, around 2.3 and 3.2 cm. Thus, radiation transfer in such glassmelts could not be regarded as a diffusion process. Instead, combined conductive and radiative heat transfer governed by Equations (1–3) should be considered. In addition, large jumps could be observed in the effective thermal conductivities $k_{eff}(T)$ for different furnace temperatures for compositions 3 [Figs. 6(a), 4 and 7(a)]. This was due to the fact that the radiative thermal conductivity $k_r(T)$ contributes the most to $k_{eff}(T)$ for compositions 3 and 4 and was sensitive to the retrieved values of κ_1 and κ_2.

Figure 7(b) shows the two-band absorption coefficient κ_1 and κ_2 in the spectral bands 0–2.8 μm and 2.8–5.0 μm retrieved for different furnace temperatures along with the spectral absorption coefficient κ_λ reported by Rubin[23] for low-iron soda-lime silicate glass. It indicates that the retrieved values of κ_1 and κ_2 were consistent from one furnace temperature to another. Their respective average value was equal to $\overline{\kappa}_1 = 30.7$ m^{-1} and $\overline{\kappa}_2 = 476.2$ m^{-1}, respectively. The retrieved value of $\overline{\kappa}_1$ was larger than that reported by Rubin.[23] whereas $\overline{\kappa}_2$ was similar to those retrieved for the three other compositions and reported in Ref. [23].

Figure 8 compares the experimentally measured temperature profile with those numerically predicted by accounting for combined conduction and radiation using the retrieved parameters summarized in Table IV for furnace temperature T_f of (a) 1300°C and (b) 1500°C. The numerical predictions agree very well with the experimental data and the nonlinear temperature profile was accurately captured. Similar results were obtained for other furnace temperatures (see Fig. S10 in Supplementary Materials).

V. Discussion

Figure 9(a) summarizes the true thermal conductivity retrieved for the four types of soda-lime silicate glassmelts with iron content ranging from 0.008 to 1.1 wt% for temperature between 1100°C and 1550°C. It indicates that the retrieved true thermal conductivity $k_c(T)$ was independent of

Table IV. Retrieved Parameters for Low-Iron Soda-Lime Glassmelt (composition 4) for Furnace Temperature T_f Between 1300°C and 1500°C

	Retrieved parameters					
Set furnace temperature T_f (°C)	$T_{f,R}$ (°C)	a (W/m·K)	b (W/m·K^2)	κ_1 (m^{-1})	κ_2 (m^{-1})	Fitness, F
1300	1284	1.26	4.59×10^{-4}	33.0	464.7	4.48×10^{-4}
1350	1335	1.64	3.92×10^{-4}	30.4	457.3	9.21×10^{-4}
1400	1385	1.19	7.99×10^{-4}	27.5	475.3	7.50×10^{-4}
1450	1438	1.06	6.35×10^{-4}	33.0	474.6	8.00×10^{-4}
1500	1490	1.03	9.19×10^{-4}	29.8	509.1	5.25×10^{-4}

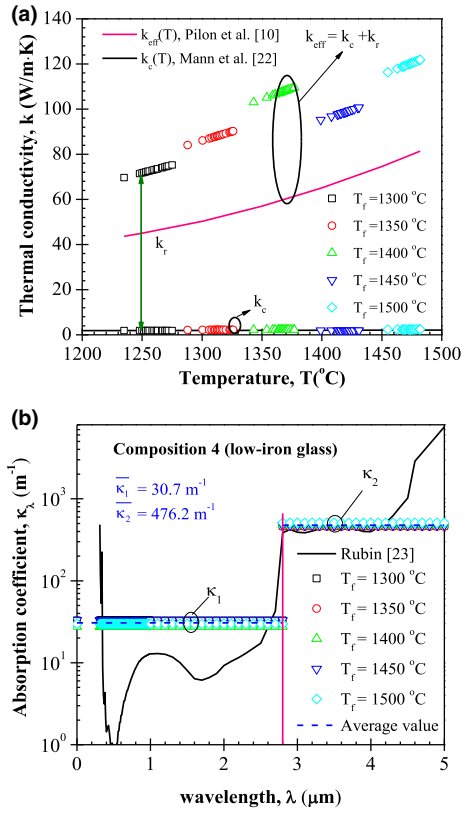

Fig. 7. Retrieved (a) true and effective thermal conductivities and (b) absorption coefficient of low-iron soda-lime silicate glassmelt (composition 4) for furnace temperature between 1300°C and 1500°C. Also shown are (i) the prediction of $k_c(T)$ from Ref. [22] (ii) the prediction of $k_{eff}(T)$ for low-iron glass from Ref. [10], and (iii) the experimental data of κ_λ for low-iron glass from Ref. [23].

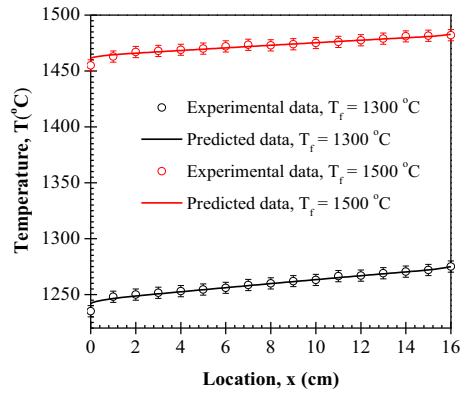

Fig. 8. Comparison between experimentally measured and numerically predicted temperature profiles using the retrieved properties reported in Table IV for low-iron soda-lime silicate glassmelt (composition 4) at furnace temperature T_f of 1300°C and 1500°C.

content and agreed relatively well with the formula reported by Mann et al.[22] for soda-lime silicate glass between 240°C and 500°C. The data retrieved between 1100°C and 1550°C can also be least-square fitted as a linear function of temperature T (in °C) given by

$$k_c(T) = 1.31 + 5.90 \times 10^{-4} T \quad (14)$$

Figure 9(b) shows the average value and the standard deviation of the retrieved two-band absorption coefficients $\overline{\kappa}_1$ and $\overline{\kappa}_2$ as a function of iron content for different furnace

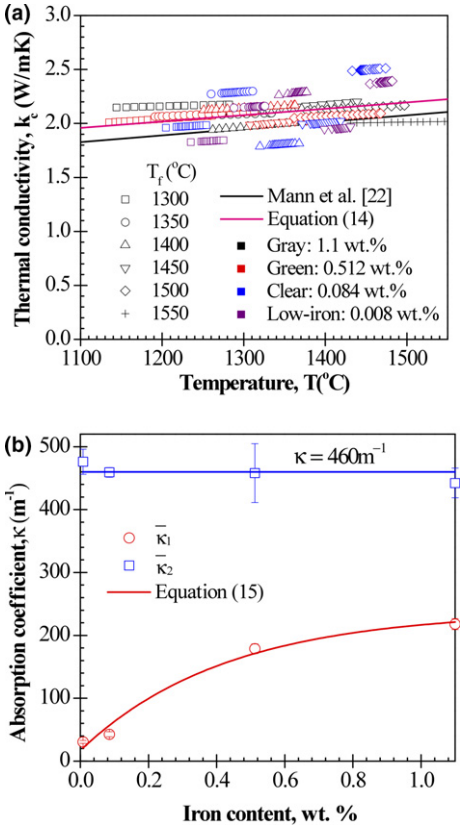

Fig. 9. Retrieved (a) true thermal conductivities and (b) two-band absorption coefficients of soda-lime silicate glass with different iron content ranging from 0.008 to 1.1 wt% and furnace temperature between 1300°C and 1550°C. Also shown are the predictions of $k_c(T)$ from Eq. (14) and from Ref. [22].

temperatures. Figure 9(b) indicates that the iron content of soda-lime silicate glassmelt γ (in wt%) affects strongly the average absorption coefficient $\overline{\kappa}_1$ in the spectral band 0–2.8 μm. Indeed, the value increased from 30.7 to 218.0 m^{-1} as the glassmelt iron content increased from 0.008 to 1.1 wt %. It can be fitted as a function of iron content γ (in wt%) as

$$\overline{\kappa}_1(\gamma) = 238 - 221\, e^{-\gamma/0.428} (\text{in m}^{-1}) \quad (15)$$

On the other hand, the absorption coefficient $\overline{\kappa}_2$ in the wavelength band 2.8–5.0 μm was found to be independent of iron content and equal to 460 ± 15 m^{-1}. These results are qualitatively consistent with data reported by Rubin.[23] It is interesting to note that the average bandwise Rosseland absorption coefficient $\overline{\kappa}_{R,2}$ computed in Section III(4) for gray and low-iron soda-lime silicate glassmelts was 474 m^{-1}.

VI. Conclusion

This paper presented an inverse analysis for retrieving (i) the true thermal conductivity $k_c(T)$ and (ii) the two-band absorption coefficient κ_1 and κ_2 of soda-lime silicate glassmelts with iron content ranging from 0.008 to 1.1 wt% from experimentally measured steady-state temperature profiles. The true thermal conductivity of soda-lime glassmelt can be considered to be independent of iron content and was given by $k_c(T) = 1.31 + 5.90 \times 10^{-4} T$, where T is given in °C and ranges between 1100°C and 1500°C. The average absorption coefficient $\overline{\kappa}_1$ for the spectral band 0–2.8 μm was strongly dependent on iron content of the glassmelt and captured by an exponential function [Eq. (15)]. On the other hand, the average absorption coefficient $\overline{\kappa}_2$ in the spectral band 2.8–

5.0 μm was independent of iron content and equal to $460 \pm 15\ m^{-1}$, which was consistent with data reported in the literature.[23]

Acknowledgment

H. Liu gratefully acknowledges the financial support of the China Scholarship Council (CSC).

Supporting Information

Additional Supporting Information may be found in the online version of this article:

Table S1. The true and retrieved input parameters from numerically generated temperature profiles predicted from the combined conduction and radiation heat transfer model for different data sets of a, b, κ_1, κ_2, and $T_{f,R}$.

Figure S1. (a) Spectral absorption coefficient of gray and low-iron glass reported in the literature [23] as well as the corresponding band coefficients used to predict steady-state temperature profile in the glassmelts; (b) the predicted steady-state temperature profiles in the gray and low-iron glassmelts slab for various cut-off wavelength of $\lambda_{cut} = 5$ and 8 μm and for furnace temperature $T_f = 1400°C$.

Figure S2. Estimated spectral normal emissivity of the crucible wall based on the optical properties of various soda-lime silicate glass reported in the literature [23] and the optical properties of alumina (the crucible was made of ~97% alumina) reported in the literature [29].

Figure S3. Spectral absorption coefficient of (a) float/clear glass and (b) green glass reported in Ref. [23] as well as the corresponding eight bands approximation of absorption coefficient used in the present study.

Figure S4. Comparison between the predicted steady-state temperature profiles and the results reported by Lee and Viskanta [24], (a) float/clear glass, and (b) green glass.

Figure S5. Spectral absorption coefficient of gray and low-iron glass reported in Ref. [23] and the corresponding band-wise Rosseland mean two-band absorption coefficient ($\kappa_{R,1}$, $\kappa_{R,2}$) defined by Eq. (12).

Figure S6. Comparison of the temperature profiles predicted by using either the spectral absorption coefficient [23] or the two-band Rosseland mean absorption coefficient approximation for (a) gray and (b) low-iron soda-lime silicate glass for $T_f = 1400°C$.

Figure S7. Comparison between experimental data and numerical temperature profiles predicted using the retrieved properties reported in Table I for gray soda-lime silicate glassmelt (composition 1) at furnace temperature T_f of (a) 1350°C, (b) 1400°C, (c) 1450°C and (d) 1500°C.

Figure S8. Comparison between experimental data and numerical temperature profiles predicted using the retrieved properties reported in Table II for green soda-lime silicate glassmelt (composition 2) at furnace temperature T_f of (a) 1300°C, (b) 1350°C, (c) 1400°C, (d) 1450°C, and (e) 1500°C.

Figure S9. Comparison between experimental data and numerical temperature profiles predicted using the retrieved properties reported in Table III for clear soda-lime silicate glassmelt (composition 3) at furnace temperature T_f of (a) 1300°C, (b) 1350°C, (c) 1400°C, (d) 1450°C, and (e) 1500°C.

Figure S10. Comparison between experimental data and numerical temperature profiles predicted using the retrieved properties reported in Table IV for low-iron soda-lime silicate glassmelt (composition 4) at furnace temperature T_f of (a) 1350°C, (b) 1400°C, and (c) 1450°C.

References

[1]T. Uchino, K. Nakaguchi, Y. Nagashima, and T. Kondo, "Prediction of Optical Properties of Commercial Soda-Lime-Silicate Glasses Containing Iron," *J. Non-Cryst. Solids*, **261** [1–3] 72–8 (2000).

[2]N. R. Paudel and Y. Yan, "Fabrication and Characterization of High-Efficiency CdTe-Based Thin-Film Solar Cells on Commercial SnO_2: F-Coated Soda-Lime Glass Substrates," *Thin Solid Films*, **549** [31] 30–5 (2013).

[3]S. V. Thomsen, K. A. Landa, R. Hulme, A. V. Longobardo, L. Landa, and A. Broughton, "Solar Cell Using low Iron High Transmission Glass with Antimony and Corresponding Method"; US Patent No. 7,770,870 B2, 2010.

[4]R. E. Field and R. Viskanta, "Measurement and Prediction of the Dynamic Temperature Distributions in Soda-Lime Glass Plates," *J. Am. Ceram. Soc.*, **73** [7] 2047–53 (1990).

[5]R. Viskanta, "Review of Three-Dimensional Mathematical Modeling of Glass Melting," *J. Non-Cryst. Solids*, **177** [2] 347–62 (1994).

[6]E. E. Anderson, R. Viskanta, and W. H. Stevenson, "Heat Transfer Through Semitransparent Solids," *J. Heat Transfer*, **95** [2] 179–86 (1973).

[7]E. E. Anderson and R. Viskanta, "Effective Thermal Conductivity for Heat Transfer Through Semitransparent Solids," *J. Am. Ceram. Soc.*, **56** [10] 541–6 (1973).

[8]M. F. Modest, *Radiative Heat Transfer*. Academic Press, San Diego, California, 2003.

[9]J. R. Howell, R. Siegel, and M. P. Mengüç, *Thermal Radiation Heat Transfer*, Taylor and Francis, New York, New York, 2011.

[10]L. Pilon, F. Janos, and R. Kitamura, "Effective Thermal Conductivity of Soda-Lime Silicate Glassmelts with Different Iron Contents Between 1100°C and 1500°C," *J. Am. Ceram. Soc.*, **97** [2] 442–50 (2014).

[11]A. Blazek and J. Endrys, "Review of Thermal Conductivity Data in Glass. Part II. Thermal Conductivity at High Temperatures"; pp. 33–100 in *International Commission on Glass*, Charleroi, Belgium, 1983.

[12]J. Endrys, A. Blazek, and J. Ederova, "Experimental Determination of the Effective Thermal Conductivity of Glass by Steady-State Method," *Glass Sci. Technol.*, **66** [6–7] 151–7 (1993).

[13]L. Kruszewski, "Total Heat-Transmission Coefficients of Amber and Green Glasses in Temperatures of Melting Range," *J. Am. Ceram. Soc.*, **44** [7] 333–9 (1961).

[14]A. Shibata, H. Suzuki, and H. Ohta, "Measurement of Thermal Transport Properties for Molten Silicate Glasses at High Temperatures by Means of a Novel Laser Flash Technique," *Mater. Trans.*, **46** [8] 1877–81 (2005).

[15]H. Ohta, H. Shibata, and T. Kasamoto, "Estimation of Heat Transfer of a Front-Heating Front-Detection Laser Flash Method Measuring Thermal Conductivity for Silicate Melts at High Temperatures," *ISIJ Int.*, **46** [3] 434–40 (2006).

[16]H. Hasegawa, H. Ohta, H. Shibata, and Y. Waseda, "Recent Development in the Investigation on Thermal Conductivity of Silicate Melts," *High Temp. Mater. Processes*, **31** [4–5] 491–9 (2012).

[17]A. F. Van Zee and C. I. Babcock, "A Method for the Measurement of Thermal Diffusivity of Molten Glass," *J. Am. Ceram. Soc.*, **34** [8] 244–50 (1951).

[18]K. Kiyohashi, N. Hatakawa, S. Aratani, and H. Masuda, "Thermal Conductivity of Heat Absorbed Soda-Lime-Silicate Glasses at High Temperatures," *High Temp. - High Pressures*, **34** [2] 127–252 (2002).

[19]J. Endrys and D. Turzik, "Die Temperaturverteilung in Glas bei Stationerem Zustand, in 9", Internationale Baustoff-und Silikattagung Weimar, Sektion 5, Hochschule für Architektur und Bauwesen, Weimar, 35–40 (1985).

[20]S. André and A. Degiovanni, "A Theoretical Study of the Transient Coupled Conduction and Radiation Heat Transfer in Glass: Phonic Diffusivity Measurements by the Flash Technique," *Int. J. Heat Mass Transfer*, **38** [18] 3401–12 (1995).

[21]M. Lazard, S. André, and D. Maillet, "Diffusivity Measurement of Semi-Transparent Media: Model of the Coupled Transient Heat Transfer and Experiments on Glass, Silica Glass and Zinc Selenide," *Int. J. Heat Mass Transfer*, **47** [3] 477–87 (2004).

[22]D. Mann, R. E. Field, and R. Viskanta, "Determination of Specific Heat and True Thermal Conductivity of Glass from Dynamic Temperature Data," *Wärme-und Stoffübertragung*, **27** [4] 225–31 (1992).

[23]M. Rubin, "Optical Properties of Soda Lime Silica Glasses," *Solar Energy Mater.*, **12** [4] 275–88 (1985).

[24]K. H. Lee and R. Viskanta, "Comparison of the Diffusion Approximation and the Discrete Ordinates Method for the Investigation of Heat Transfer in Glass," *Glass Sci. Technol.*, **72** [8] 254–65 (1999).

[25]K. H Lee and R. Viskanta, "Two-Dimensional Combined Conduction and Radiation Heat Transfer: Comparison of the Discrete Ordinate Method and the Diffusion Approximation Methods," *Numer. Heat Transfer, Part A*, **39** [3] 205–25 (2001).

[26]M. Mitchell, *An Introduction to Genetic Algorithms*. MIT Press, Cambridge, Massachusetts, 1996.

[27]L. Gosselin, M. Tye-Gingras, and F. Mathieu-Potvin, "Review of Utilization of Genetic Algorithms in Heat Transfer Problems," *Int. J. Heat Mass Transfer*, **52** [9–10] 2169–88 (2009).

[28]D. Lacroix, N. Berour, P. Boulet, and G. Jeandel, "Transient Radiative and Conductive Heat Transfer in Non-Gray Semitransparent Two-Dimensional Media with Mixed Boundary Conditions," *Heat Mass Transf.*, **42** [4] 322–37 (2006).

[29]O. B. Toon and J. B. Pollack, "The Optical Constants of Several Atmospheric Aerosol Species: Ammonium Sulfate, Aluminum Oxide, and Sodium Chloride," *J. Geophys. Res.*, **81** [33] 5733–48 (1976). □